Monoterpenes oxidation in the presence of Y zeolite-entrapped manganese(III) tetra(4-*N*-benzylpyridyl)porphyrin

F.C. Skrobot [b], A.A. Valente [a], G. Neves [a], I. Rosa [b],
J. Rocha [a,*], J.A.S. Cavaleiro [a]

[a] *Department of Chemistry, University of Aveiro, 3810-193 Aveiro, Portugal*
[b] *Department of Chemistry, UFSCar, Via Washington Luiz, Km 235, CEP, 13565-905 São Carlos, SP, Brazil*

Abstract

Under homogeneous conditions and as a Y zeolite supported complex, manganese(III) tetra(4-*N*-benzylpyridyl)porphyrin (MnTBzPyP) is an active catalyst in the epoxidation of (R)-(+)-limonene and α-pinene, and in the hydroxylation of carvacrol and thymol, using H_2O_2/ammonium acetate, at room temperature and atmospheric pressure. A combined study on the characterization and catalytic performance of MnTBzPyP–NaY suggests that its preparation led to a successful inclusion of MnTBzPyP inside the zeolite during the hydrothermal synthesis. Unfortunately, irreversible catalyst deactivation occurs in the presence of H_2O_2. Changes in the crystalline structure of MnTBzPyP–NaY during the oxidative transformations are accompanied by leaching of the porphyrin complex to the reaction solution, accounting for the nearly complete loss of activity when the catalyst is re-used. Higher substrate conversions were achieved with the zeolite-impregnated complex. The iron analogue is inactive, under the applied reaction conditions.
© 2003 Elsevier Science B.V. All rights reserved.

1. Introduction

Synthetic metalloporphyrins have been intensively investigated to mimic the activity of enzymatic monoxygenases. Such porphyrin systems can catalyze alkane hydroxylation and alkene epoxidation using single oxygen atom donors such as iodosylbenzene, hypochlorites and hydroperoxides [1]. They can also dismute peroxides (catalase-like function), which is a competitive reaction in the oxidation of the substrate (oxygenase-like function) ([2] and references

therein). Some major drawbacks are encountered when not readily available metalloporphyrin catalysts are employed in homogeneous systems. The catalyst deactivates under the operating conditions due to side reactions that lead to the formation of less reactive oxo-bridged dimer/oligomer compounds and of metal species with an intermediate oxidation state, which cannot re-enter the oxidation cycle, leading to rather low turnover numbers [3–6]. Such problems have been addressed through the use of high substrate/oxidant ratios and the development of sterically hindered metalloporphyrins by introducing bulky substituents at the peripheral *meso-* and β-positions of the macrocycle ring in order to restrict deleterious intermolecular reactions and increase the oxidative

* Corresponding author. Tel.: +351-34-370330;
fax: +351-34-370084.
E-mail address: corocha@dq.ua.pt (J. Rocha).

stability of the ligand [7–13]. Further progress has
been made through the immobilization of the com-
plexes on solid supports to control the local environ-
ment of the oxidation and to aid catalyst recovery
and re-use [14–19]. One of the methods that attracted
much attention for site isolation of the metal active
species consists on the hydrothermal synthesis of
faujasite type zeolites (which are largely used for pro-
cessing petrochemicals) in the presence of cationic
metalloporphyrins, sometimes referred to as the
"build-bottle-around-ship" approach [20–22]. In such
hybrid catalysts the dimensions of the guest molecules
are larger than those of the zeolitic nanocages and
are, therefore, physically trapped inside the inorganic
host. The electrostatic interactions between the an-
ionic aluminosilicate support and the cationic guest
molecules contribute to the successful inclusion of the
complexes.

Metalloporphyrin systems are of considerable in-
terest for sophisticated organic synthesis to high-value
products, such as fine chemicals. Monoterpenes are
widely used in pharmaceutical, cosmetic and food
industries as active components and the synthetic
routes often involve epoxides or alcohols as in-
termediates [23]. Some reactions of considerable
commercial importance are: epoxidation of α-pinene
to α-pinene oxide, which is an intermediate used in
the synthesis of several sandalwood fragrances [24];
epoxidation of limonene to limonene oxide, used to
treat rhinitis [25]; oxidation of carvacrol or thymol
to thymoquinone, which has antitumor and hepato-
protective effects [26a,b]. Preliminary studies showed
that, under homogeneous conditions, the readily
available manganese(III) 5,10,15,20-tetrakis(4-N-
methylpyridyl)porphyrin is inactive in the oxidation
of the previously mentioned monoterpenes and no
activity was gained with its heterogenization (with
the hydrothermal synthesis of Y zeolite). This is not
surprising since this porphyrin complex bound to
novel bis-fuctionalized silica gives <0.5% conversion
of (Z)-cyclooctene (a rather reactive substrate) after
24 h [27]. When Mn(III) porphyrins are designed
with bulkier substituents they become quite efficient
homogeneous catalysts for oxidizing monoterpenes,
under mild conditions using H_2O_2 as oxidant and
ammonium acetate as co-catalyst [28,29]. Hydrogen
peroxide is an inexpensive and environmental friendly
oxidant since H_2O is its reduction product. Ammo-
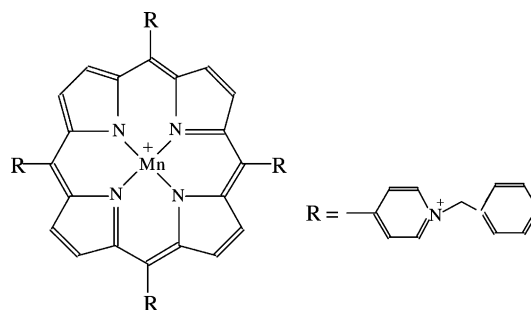
Scheme 1. Mn(III) 5,10,15,20-tetra(4-N-benzylpyridyl)porphyrin (MnTBzPyP).

nium acetate is known to act as a very efficient, stable
and inexpensive co-catalyst for Mn(III) porphyrin
catalyzed oxygenations by H_2O_2 [30].

Here, we wish to report the synthesis of Y zeolite in
the presence of Mn(III) tetra(4-N-benzylpyridyl)por-
phyrin, which was characterized by a wide range of
techniques, uncommonly found in related studies re-
ported in the literature. The catalytic activity of the
free and immobilized complexes is studied for epox-
idation and hydroxylation processes of monoterpenes
using H_2O_2/ammonium acetate. A detailed study on
the catalysts stability under the operating conditions
has also been carried out.

2. Experimental

2.1. Catalyst preparation

The synthesis of the Mn(III) tetra(4-N-benzylpyri-
dyl)porphyrin (MnTBzPyP, Scheme 1) is described
elsewhere [31]. Zeolite-Y was synthesized in the pres-
ence of MnTBzPyP (MnTBzPyP–NaY) according to
a procedure already reported [20,21] for the inclu-
sion of cationic metalloporphyrins inside nanocages
of faujasites X and Y during hydrothermal synthesis.
The complexes adsorbed on the external surface of the
as-synthesized zeolite were removed through Soxh-
let extractions with distilled water (72 h), methanol
and 1,2-dichloroethane (24 h each). Zeolite-NaY was
prepared in the same way, but without the addition
of porphyrin. A sample was prepared by impreg-
nation of proportional amounts of MnTBzPyP on
NaY (NaY–MnTBzPyP_{imp}) and this was followed by

evaporation of the solvent (dichloromethane) at room temperature.

2.2. Catalyst characterization

Powder X-ray diffraction (XRD) of the samples was carried out on a Philips X'Pert MPD diffractometer using Cu Kα X-radiation. Variable temperature in situ powder XRD was carried out using an Anton Parr high-temperature chamber. Scanning electron microscopy (SEM) and energy dispersive X-ray spectrometry (EDS) were carried out on a Hitachi S-4100 microscope. Atomic absorption analysis was performed on a Perkin-Elmer A Analyst 100 instrument. The TGA and DSC curves were measured using TGA-50 and DSC Shimadzu analyzers, respectively. The samples were heated at $5°$/min until $500°C$ under air and kept at this temperature for 10 min. Nitrogen adsorption isotherms were measured at 77 K, using a gravimetric adsorption apparatus equipped with a CI electronic MK2-M5 microbalance and an Edwards Barocel pressure sensor. Before the measurements, the molecular sieves were outgassed at $120°C$ (to minimize destruction of the functionalities) and maintained at this temperature overnight to a residual pressure of ca. 10^{-4} mbar. The texture parameters, Langmuir specific surface area (S_{Lang}) and specific total pore volume (V_p) are estimated from the adsorption isotherm data. UV-Vis spectroscopy was performed on a Jasco V-560 PC instrument. The MnTBzPyP–NaY sample was treated with concentrated nitric acid to destroy the inorganic framework before recording the UV-Vis spectra. No demetallation was observed for the organic macrocycle. The complex loading was estimated using a calibration curve measured with MnTBzPyP. Diffuse-reflectance UV-Vis was recorded on the same instrument using $BaSO_4$ as the reference material. The IR spectra were measured on a Unican Mattson Mod 7000 FTIR spectrometer using KBr pellets. Raman spectra were recorded on a Bruker RFS 100/S FT Raman spectrometer using a 1064 excitation of the Nd/YAG laser. ^{27}Al solid-state magic angle spinning NMR spectra were recorded at 104.3 MHz on a Bruker Avance 400 spectrometer, with $9°$ pulses, a spinning rate of 13.5 kHz and 1 s recycle delays; ^{29}Si MAS NMR spectra were recorded at 79.49 MHz, with $40°$ pulses, a spinning rate of 5 kHz and 35 s recycle delay.

2.3. Catalytic reactions

The oxidations of α-pinene, (R)-(+)limonene, carvacrol and thymol were carried out at $25°C$ and atmospheric pressure using hydrogen peroxide as the oxygen-atom donor: 0.1 mmol H_2O_2 was added each 30 min (until a total of 1 mmol, method A) to the reaction mixture composed of 1 mmol monoterpene, 250 μl acetonitrile as solvent, 0.13 mmol ammonium acetate, 20 mg supported or 0.01 mg free metalloporphyrin. An experiment was carried out by adding 0.5 mmol hydrogen peroxide each 15 min until a total of 4 mmol (method B). Gas chromatographic analyses were carried out on a Varian 3800 GC, equipped with a SPB-5 capillary column (25 m × 0.25 mm × 0.25 μm) and a FID detector. The oxidation products were characterized by using a HP 5970 GC–MS.

3. Results

3.1. Catalyst characterization

The light brown color of the powder obtained after the extensive Soxhlet extractions, designated as MnTBzPyP–NaY, suggests the successful entrapment of the Mn(III) porphyrin inside the zeolite. In comparison to other porphyrin complexes reported in literature (for example, tetrakis(N,N,N-trimethylanilinium) porphyrin, [20]; tetraphenylporphyrin, [32]) the distance across two opposite benzylpyridyl substituents of MnTBzPyP (assuming a planar macrocycle ring) is expected to be at least 18 Å. Hence, for the complex to be accommodated inside the zeolitic cages (13 Å diameter), changes in the conformational geometry of the porphyrin moiety are required so that the benzyl units may protrude through the four 12-ring windows.

The SEM image and powder XRD pattern of MnTBzPyP–NaY are similar to those observed for NaY, indicating that they possess the same morphology and crystalline structures, i.e. the framework around the guest molecule MnTBzPyP is faujasite-Y (Figs. 1 and 2). The same is observed for NaY–MnTBzPyP$_{imp}$, suggesting that the solid support is structurally unchanged and manganese porphyrin should be dispersed molecularly on the external surface.
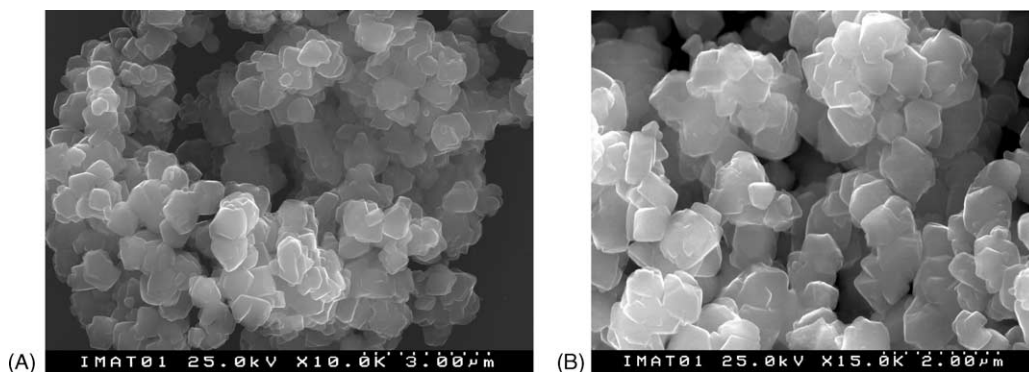
Fig. 1. SEM images of NaY (A) and MnTBzPyP–NaY (B).

The ^{27}Al MAS NMR spectra of the three molecular sieve samples exhibit a signal at ca. 60 ppm ascribed to tetrahedrally coordinated framework aluminum (not shown) [33]. The spectrum of MnTBzPyP–NaY showed two additional very small peaks centered at ca. 0 and 13 ppm, which may be assigned to octahedral non-framework Al species formed during the hydrothermal synthesis of the zeolite around the Mn(III) porphyrin complex.

The Si/Al ratio of the three samples is ca. 2.2, ascertained by EDS. The values calculated from the ^{29}Si MAS NMR spectral intensities are 2.5 for NaY and 1.6 for MnTBzPyP–NaY. The latter value is the same as that reported by Zhan and Li [20] for metallopor-

phyins encapsulated in zeolite-Y prepared by the same synthesis method. The ^{29}Si MAS NMR spectrum of MnTBzPyP–NaY showed a slightly raised base line, suggesting the presence of some amorphous silica in the sample, which may account for the higher ratio of Si/Al obtained by EDS (2.2).

Atomic absorption analysis of MnTBzPyP–NaY gives 0.03 wt.% Mn loading, corresponding to 5.4 μmol of complex per gram, which is the same as that obtained by UV-Vis using a calibration curve. The UV-Vis spectrum of MnTBzPyP–NaY is similar to that of its homogeneous counterpart, showing four main bands that appear at approximately 360, 385, 455 (Soret) and 545 nm (Fig. 3). These results suggest
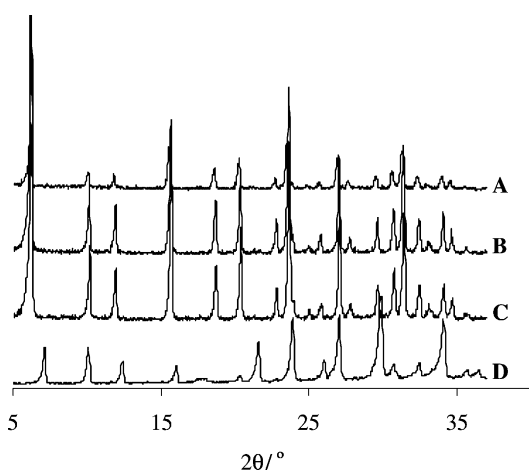

Fig. 2. Powder XRD patterns of NaY (A), NaY–MnTBzPyP$_{imp}$ (B), MnTBzPyP–NaY before (C) and after reaction (D).
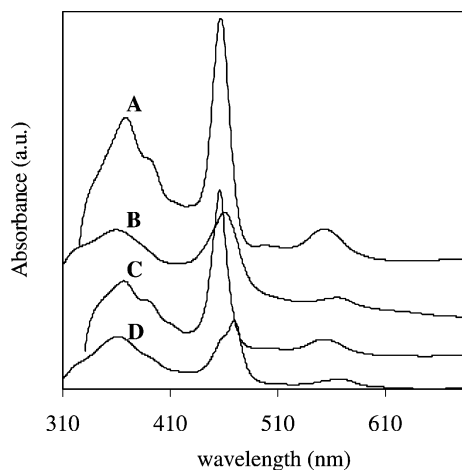

Fig. 3. UV-Vis spectra of MnTBzPyP–NaY treated with HNO$_3$ (A) or H$_2$O$_2$ (B), reaction solution of terpene oxidation after the removal of the solid (C), MnTBzPyP dissolved in HNO$_3$ (D).

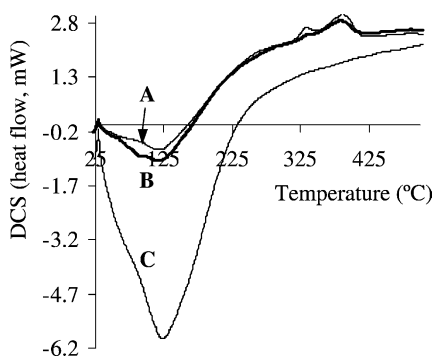Fig. 4. DSC analysis of MnTBzPyP–NaY (A), NaY–MnTBzPyP$_{imp}$ (B) and NaY (C).

Fig. 5. FTIR spectra of MnTBzPyP (A), NaY (B), NaY–MnTBzPyP$_{imp}$ (C), MnTBzPyP–NaY (D).

that no significant demetallation or no metal ion exchange took place during the synthetic procedure.

DSC curves of MnTBzPyP–NaY and NaY–MnTBzPyP$_{imp}$ show two small exothermic bands in the temperature range 300–400 °C, which do not appear for zeolite-Y, suggesting that they arise from the decomposition of the Mn(III) porphyrin complex (Fig. 4). Indeed, the DSC analysis of MnTBzPyP gives a broad exothermic band with an onset at ca. 300 °C. The zeolite samples show a broad endothermic band at 50–200 °C, which may be assigned to water loss [34]. The water and organic mass loss of MnTBzPyP–NaY may be estimated from the TGA curve (for the corresponding temperature intervals) as 21 and 1.2% of the initial mass, respectively. Assuming that the sample is only composed of framework silicate and aluminate (with Si/Al ratio of 2.2), sodium cations, water and tetracationic porphyrin, the calculated average unit cell composition is Na$_{59.2}$(MnTBzPyP)$_{0.2}$[(AlO$_2$)$_{60}$(SiO$_2$)$_{132}$]·190H$_2$O. This gives an estimated occupation of approximately one porphyrin per 40 supercages. The complex loading level is similar to that reported in literature for faujasite-Y encapsulated metallotetrakis(N,N,N-trimethylanilinium) prepared in a similar fashion (the same Si/Al ratio was also obtained, as mentioned above) [20]. It is noteworthy that the unit cell composition corresponds to a Mn loading of ca. 0.07 wt.%, which is higher than that estimated by UV-Vis (0.03 wt.%). This might be due to an overestimation of the organic mass loss from the TGA curve.

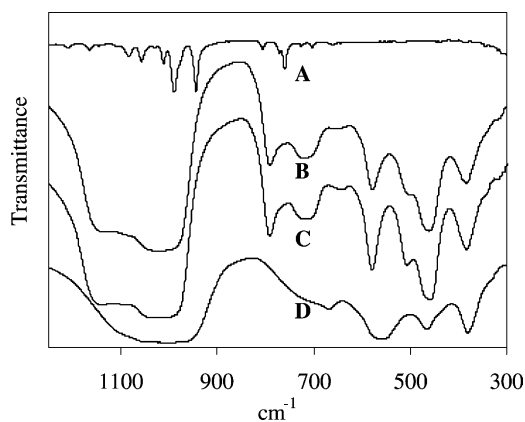The diffuse-reflectance UV-Vis and FT Raman spectra of NaY, MnTBzPyP–NaY and NaY–MnTBzPy

P$_{imp}$ are similar (not shown). The spectra of MnTBzPyP is masked by the zeolite bands due to the low concentration of the former. The FTIR spectrum of MnTBzPyP–NaY shows some differences from that of NaY and NaY–MnTBzPyP$_{imp}$ in the region 420–820 cm^{-1}, which may result from slight changes in the overall structure upon the synthesis of the anionic aluminosilicate framework around the tetracationic MnTBzPyP (Fig. 5). The unsuccessful characterization of the samples by X-ray photoelectron spectroscopy was due to the low Mn loading level.

The N$_2$ adsorption isotherms of the three zeolitic samples are of Type I, characteristic of microporous solids. The values of the texture parameters of NaY, determined from the adsorption isotherm, are in agreement with data from known literature [34]: $S_{Lang} = 854$ m^2 g^{-1} and $V_p = 0.30$ cm^3 g^{-1}. The isotherms show a decreasing N$_2$ uptake upon immobilization of the MnTBzPyP complex. The values of the surface area and total pore volume of NaY decreased ca. 17% upon encapsulation (Table 1). Assuming that each guest molecule in MnTBzPyP–NaY occupies the total volume of one cage with a diameter of 13 Å, the decrease of V_p can be estimated as ca. 13%, which is close to that determined from the N$_2$ adsorption data (17%). Impregnation of MnTBzPyP on the external surface of the zeolite led to a drastic decrease (ca. 97%) of S_{Lang} and V_p. These results suggest that the impregnated porphyrin complex blocks the open pores, i.e. cavities or channels with access to the surface. Assuming that the distance across two opposite

Table 1
Texture parameters of Y zeolite samples from N_2 adsorption isotherms at 77 K

Sample	S_{Lang} $(m^2 g^{-1})$	ΔS_{Lang}[a] (%)	V_P $(cm^3 g^{-1})$	ΔV_P[b] (%)
NaY	854	–	0.30	–
MnTBzPyP–NaY	712	−17	0.25	−17
NaY–MnTBzPyP$_{imp}$	16	−98	0.01	−97

[a] Variation of surface area in relation to NaY sample.
[b] Variation of the total pore volume in relation to NaY sample.

peripheral groups of the planar metalloporphyrin is 18 Å (at least), it may be estimated that 5.4 μmol complex adsorbed on the external surface as a monolayer would cover approximately $53 m^2/g$ of zeolite, which is quite significant.

The diffraction peaks of these molecular sieves were indexed on cubic unit cells and the Rietveld refined lattice constants (error was always <0.01 Å) as a function of temperature are shown in Fig. 6. The influence of the temperature on the inorganic lattice is similar for MnTBzPyP–NaY and NaY, showing a slight contraction of the framework at $100\,^{\circ}C$ most likely due the dehydration of the molecular sieves. The fact that the lattice constant of MnTBzPyP–NaY is higher than that of NaY suggests that the framework of the former is slightly more expanded due to the nanoinclusion of the Mn(III) porphyrin complex. Above $150\,^{\circ}C$ the lattice constant of the impregnated sample is roughly
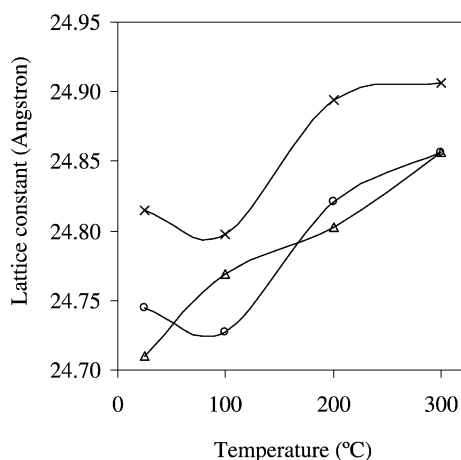

Fig. 6. Influence of the temperature on the lattice constant of NaY (○), MnTBzPyP–NaY (×), and NaY–MnTBzPyP$_{imp}$ (△).

the same as that of NaY. However, contrary to what is observed for other molecular sieves, the lattice constant of NaY–MnTBzPyP$_{imp}$ increased upon heating to $100\,^{\circ}C$, suggesting that the impregnated porphyrin somehow "disturbed" the framework structure, which is surprising since the complex is adsorbed on the external surface of the zeolite. It is possible that a significant amount of water (vapor) desorbed upon dehydration becomes trapped inside the aluminosilicate support by the impregnated complexes, which block the pore openings on the external surface (according to the N_2 adsorption data), leading to a slight expansion of the framework.

It is worthy of mentioning that no significant loss of crystallinity was observed for NaY and NaY–MnTBzPyP$_{imp}$ upon heating to $400\,^{\circ}C$, whereas the MnTBzPyP–NaY sample showed significant loss of crystallinity upon heating above $300\,^{\circ}C$, the temperature at which the porphyrin moiety is decomposed.

3.2. Oxidation of monoterpenes

The catalytic performance of MnTBzPyP–NaY was studied for the oxidation of monoterpenes, (R)-$(+)$-limonene, α-pinene, carvacrol and thymol, using H_2O_2/NH_4CH_3COO, acetonitrile as solvent, at $25\,^{\circ}C$ and atmospheric pressure. The catalytic results are compared with the analogous homogeneous system. Control experiments showed that Y zeolite is inactive, under the operating conditions.

Both homogeneous and heterogenized Mn(III) porphyrin complexes are active in the oxidation of all the monoterpenes under study as long as ammonium acetate is present. Many studies have shown that Mn(III) porphyrins are active catalysts for liquid phase oxidation with H_2O_2 when a co-catalyst is used, which is thought to facilitate the heterolytic cleavage of the peroxide bond and to stabilize the porphyrin metal-oxo active species [1,5,15,30,35–37].

The kinetic curves of MnTBzPyP–NaY are similar to those observed for the homogeneous counterpart, suggesting that the reaction takes place through a similar mechanism (Fig. 7). The oxidation rates of the terpenes with MnTBzPyP–NaY are, in general, slightly higher than in homogeneous phase. Initial activities vary between $3.2\,mol\,mol_{Mn}^{-1}\,min^{-1}$ for carvacrol and $39.4\,mol\,mol_{Mn}^{-1}\,min^{-1}$ for α-pinene oxidation and turnover numbers (at 6 h) are rather high varying
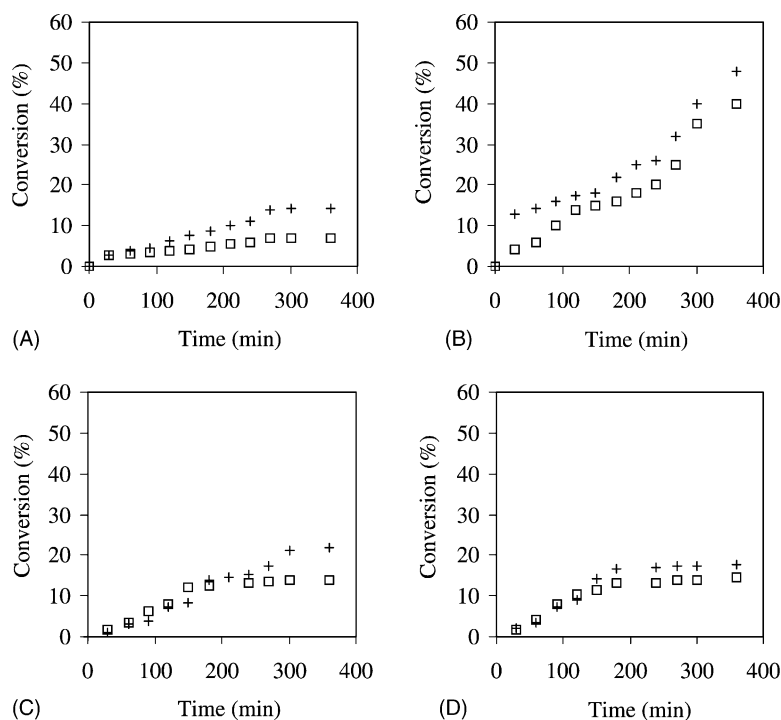
Fig. 7. Kinetic curves of limonene (A), α-pinene (B), carvacrol (C) and thymol (D) oxidations in the presence of MnTBzPyP–NaY (+) or free MnTBzPyP (□).

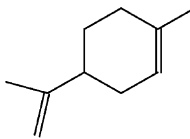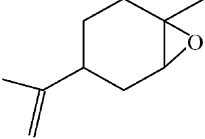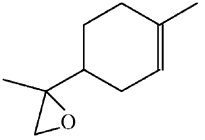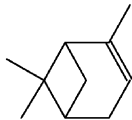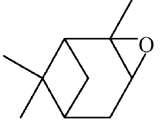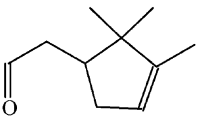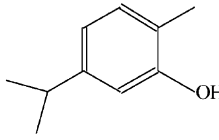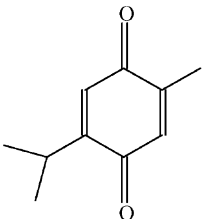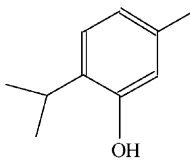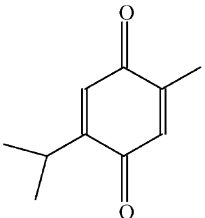between $1291\,\mathrm{mol\,mol_{Mn}^{-1}}$ for (R)-$(+)$-limonene and $4364\,\mathrm{mol\,mol_{Mn}^{-1}}$ for α-pinene oxidation (Table 2). The porphyrin catalysts give 40–50% α-pinene conversion within 6 h of reaction at room temperature, whereas <25% conversion is observed for the remaining substrates, even after 24 h.

In the oxidations of (R)-$(+)$-limonene and α-pinene the Mn(III) porphyrin catalysts possess mainly epoxidation activity (Table 2). The product selectivity is plotted as a function of the conversion of the substrate in Fig. 8. The oxidation of (R)-$(+)$-limonene gives limonene oxide as the main product and 8,9-epoxy-p-menth-1-ene as the only side product, these epoxides result from the oxidation of the internal trisubstituted and terminal C=C bond, respectively. It has been reported for the oxidation of monoterpenes with Mn(III) porphyrin complexes that the regioisomeric product distribution likely depends on the relative nucleophilicity of the two double bonds [28]. In the presence of the homogeneous MnTBzPyP complex, limonene oxide and 8,9-epoxy-p-menth-1-ene

are formed in an average molar ratio of ≈3 throughout the first 6 h of reaction. This value is nearly double that observed for MnTBzPyP–NaY (≈1.6), suggesting that the zeolite matrix displays size selectivity in favor of the epoxidation of the terminal C=C bond. Similar results have been reported for Ru(II) porphyrin complexes immobilized into mesoporous MCM-41 molecular sieves for which the above molar ratio equals 0.6 [19]. The oxidation of α-pinene in the presence of the porphyrin catalysts produces mainly α-pinene oxide. For MnTBzPyP–NaY, a pronounced decrease in epoxide selectivity with increasing α-pinene conversion is observed in detriment of the formation of campholenic aldehyde (Fig. 8). The latter product is an intermediate used for the synthesis of sandalwood fragrance santalol and may be formed by the Lewis acid catalyzed rearrangement of α-pinene oxide ([38] and references therein).

In the oxidations of carvacrol and thymol the porphyrin catalysts possess aromatic ring oxidation activity, producing thymoquinone as the only product

Table 2

Monoterpenes oxidation using H_2O_2 in the presence of the porphyrin catalysts[a]

Substrate	Initial activity[b] (mol mol$_{Mn}^{-1}$ min^{-1})	TON[c] (mol mol$_{Mn}^{-1}$)	Conversion[d] (%)	Product	Select[e] (%)
Limonene	8.2 (8.8)	1291 (627)	21 (10)		58 (65)
					42 (35)
α-Pinene	39.4 (12.1)	4364 (3636)	52 (45)		71 (48)
					21 (24)
Carvacrol[f]	3.2 (5.2)	1984 (1261)	25 (14)		100 (100)
Thymol[f]	6.3 (5.1)	1616 (1325)	18 (15)		100 (100)

[a] Results in brackets are for the homogeneous phase oxidation in the presence of MnTBzPyP.

[b] Calculated as (mol converted terpene/(mol MnTBzPyP × 30 min)).

[c] Calculated for 360 min.

[d] Converted substrate after 24 h of reaction.

[e] For α-pinene oxidation small amounts of other non-identified products are formed during the reaction.

[f] Free and Y zeolite-encapsulated 5,10,15,20-tetrakis(4-N-methylpyridyl)porphyrin was inactive.
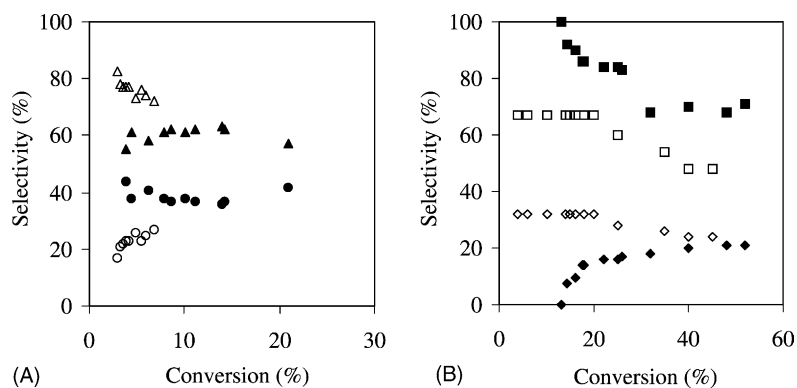
Fig. 8. Conversion versus selectivity profiles for (R)-(+)-limonene (A) and α-pinene (B) oxidations in the presence of MnTBzPyP–NaY (solid symbols) or free MnTBzPyP (open symbols): limonene oxide (△); 8,9-epoxy-p-menth-1-ene (○); α-pinene oxide (□); campholenic aldehyde (◇).

in up to 25% yield at 24 h (Table 2). The kinetic curves obtained for the oxidation of these substrates in homogeneous phase are practically coincident, suggesting that they have similar reactivity (Fig. 7). The same has been reported for several Mn(III) and Fe(III) porphyrin catalysts, under similar reaction conditions [29,39]. According to the literature, the quinone may result from the oxidation of a hydroquinone intermediate ([29,39,40] and references therein).

It is noteworthy that for all the substrates the heterogenized Mn(III) porphyrin catalyst shows a similar behavior to the homogeneous analogue since in both cases the reaction after 6 h proceeds at a much lower rate accounting for a minor increase in conversion until 24 h. Furthermore, terpene conversions after 24 h are still far from quantitative, even though the reaction was performed adding an equivalent amount of H_2O_2 to the substrate. This may be attributed to the wasteful consumption of the oxidant, resulting in poor oxygen transfer to the organic substrate. This can also be caused by the competitive oxidation of acetonitrile, used as solvent [13,41,42]. However, no products resulting from the oxidation of acetonitrile were detected. The deactivation of the catalysts may also account for the observed results. An excess of H_2O added together with the oxidant may inhibit the reaction by converting the active metal species in less reactive/inactive species [13]. However, when the H_2O_2 (30% aqueous) solution is substituted by proportional amounts of an anhydrous source of H_2O_2, namely urea–hydrogen peroxide adduct, carvacrol conversion

at 6 and 24 h reaction is the same (23%). These results suggest that catalytic deactivation due to the presence of H_2O is not significant.

In the homogeneous phase the color of the reaction solution changes from light to very dark brown, suggesting that the Mn(III) porphyrin complex is gradually degraded, probably due to oxidative self-destruction and aggregation The encapsulation of MnTBzPyP in Y zeolite should, in principle, minimize dimerization or catalyst intermolecular self-oxidation. The catalytic performance and stability of MnTBzPyP–NaY was further studied for carvacrol oxidation.

The gradual addition of oxidant according to method A was repeated in the second and third day for the carvacrol reaction. In homogeneous phase no carvacrol conversion was observed during the second cycle of peroxide addition, whereas in the presence of the supported porphyrin (MnTBzPyP–NaY or NaY–MnTBzPyP$_{imp}$) an increase in more than 40% of the value of conversion was observed (Fig. 9). Hence, the manganese complex when immobilized seems to be more stable in the oxidizing medium, probably due to the electrostatic interactions between the four cationic peripheral groups of the porphyrin and the anionic aluminosilicate framework. For the heterogeneous systems, the fact that the reaction continues upon the addition of more peroxide, suggests that the Mn(III) porphyrin complex possesses catalase-like activity, responsible for the non-productive decomposition of H_2O_2. The kinetic

profiles of MnTBzPyP–NaY and NaY–MnTBzPyP$_{imp}$ show no significant increment in conversion during the third cycle of peroxide addition. It is possible that the catalysts deactivate in the course of reaction with increasing H_2O_2 concentration.

The addition of a larger amount of oxidant to the reaction mixture containing MnTBzPyP–NaY (according to method B referred to in Section 2) increases significantly the initial reaction rate (from 0.02 for method A to 0.13 mmol g^{-1} min^{-1} for method B), but after 1 h no further oxidation is observed: carvacrol conversion is 14%, the same as that obtained in homogeneous phase, suggesting that an excess of H_2O_2 decreases the stability of the catalyst.

In another experiment, MnTBzPyP–NaY was separated from the reaction mixture after 24 h, washed with acetonitrile and dried at 60 °C to be re-used. In the second reaction cycle the carvacrol conversion, after 24 h was <1% indicating nearly complete loss of catalytic activity (Fig. 9). After the first run, the color of the catalyst changed from light brown to yellow and the yellow filtrate contained porphyrin (ascertained by UV-Vis spectroscopy, Fig. 3). Hence, leaching of the porphyrin complex from the zeolite to the reaction medium during the oxidative transformations leads to the loss of activity when the catalyst is recycled.

It is not clear how the Mn(III) porphyrin complex is leached from the microporous framework if all non-encapsulated Mn(III) porphyrin was removed from the zeolite during the Soxhlet extractions carried

out after the synthesis. This was further confirmed by rewashing the unused MnTBzPyP–NaY solid with acetonitrile and water. The catalyst retained its original color and the UV-Vis spectra of the recovered solvents showed no detectable amounts of complex. However, when MnTBzPyP–NaY is washed with H_2O_2 (30% aqueous) a significant amount of porphyrin complex is extracted, ascertained by UV-Vis (Fig. 3). These results suggest that H_2O_2, rather than the solvent, favors the leaching phenomenon, which explains the above results.

Powder XRD patterns of NaY, NaY–MnTBzPyP$_{imp}$ and MnTBzPyP–NaY were recorded after the reaction. Whereas no loss of crystallinity was observed for NaY and NaY–MnTBzPyP$_{imp}$, significant changes occurred in the XRD pattern of MnTBzPyP–NaY (Fig. 2). Thus, leaching of the intrazeolite porphyrin complex is accompanied by partial collapse and changes of the crystalline structure of MnTBzPyP–NaY, leading to its irreversible deactivation. These results, together with the fact that it was only for this sample that significant collapse of the crystalline structure occurred upon heating above 300 °C under air (coinciding with the decomposition of the porphyrin, ascertained by powder XRD) indicate that MnTBzPyP–NaY is less stable than NaY–MnTBzPyP$_{imp}$. This may explain the difference in activity between the encapsulated and impregnated complex observed after 250 min (Fig. 9), NaY–MnTBzPyP$_{imp}$ gives higher substrate conversions than MnTBzPyP–NaY suggesting that the latter catalyst deactivates faster than the former.

Zhan and Li [20] reported that Y zeolite confined manganese(III) tetrakis(N,N,N-trimethylanilinium) porphyrin complexes are stable catalysts towards leaching of the porphyrins to the reaction solution under oxidizing conditions using tert-butyl hydroperoxide. In the case of MnTBzPyP–NaY, the substitution of H_2O_2 for tert-butyl hydroperoxide did not solve the leaching problems. The poor stability of MnTBzPyP–NaY may be related to the fact that the porphyrin complex, which contains four (large) benzylpyridyl peripheral substituents, is very spacious and, therefore, extremely sterically hindered inside the microporous structure.

A preliminary study on the iron analogue, FeTMePyP–NaY (synthesized using the same conditions as for MnTBzPyP–NaY) showed that this
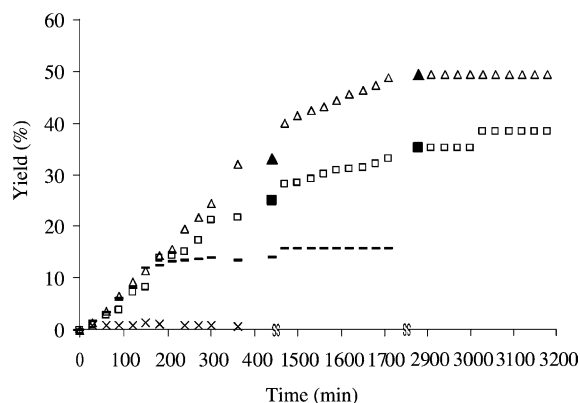

Fig. 9. Kinetic curves of carvacrol oxidation in the presence of free MnTBzPyP (−), NaY–MnTBzPyP$_{imp}$ (△), fresh (□) or recycled (×) MnTBzPyP–NaY. The solid symbols refer to the beginning of a new cycle of peroxide addition each 24 h.

catalyst is inactive for carvacrol oxidation, under the same reaction conditions. This may be explained by the propensity of the Fe(III) porphyrin to dismutate H_2O_2 rather than to oxidize the substrate under the applied reaction conditions.

4. Conclusions

The homogeneous and heterogenized MnTBzPyP complex is active in the oxidation of monoterpenes with H_2O_2/ammonium acetate, at room temperature and atmospheric pressure. The oxidation of (R)-(+)-limonene (<21% conversion, at 24 h) and α-pinene (<52% conversion) produces limonene oxide and α-pinene oxide as the main product, respectively. The oxidation of carvacrol (<25% conversion) and thymol (<18% conversion) gives thymoquinone with 100% selectivity.

A detailed study on the characterization (powder XRD, TGA, DSC, N_2 adsorption, SEM, EDS, UV-Vis, FTIR, Raman, solid state MAS NMR) and catalytic performance of MnTBzPyP–NaY suggests that its preparation led to the successful nanoinclusion of the tetracationic Mn(III) porphyrin inside the aluminosilicate framework. The goal of achieving a catalyst that is more stable than its homogeneous counterpart was partially achieved. Unfortunately, the catalyst is unstable towards leaching of the complex in the presence of H_2O_2, which accounts for nearly complete loss of activity when it is recycled. Apparently, no catalytic activity and stability is gained with the inclusion of MnTBzPyP during the synthesis of Y zeolite in relation to the zeolite-impregnated complex. Leaching of the porphyrin from MnTBzPyP–NaY occurs in the presence of H_2O_2 and is accompanied by partial collapse and changes of the crystalline structure, causing irreversible deactivation. Such instability may be related to the large dimensions of the guest molecules. The iron analogue was inactive under the same reaction conditions.

Acknowledgements

References

[1] B. Meunier, A. Robert, G. Pratviel, J. Bernadou, in: K.M. Kadish, K. M. Smith, R. Guilard (Eds.), The Porphyrin Handbook, vol. 4, Academic Press, USA, 2000, p. 119.
[2] J.-Y. Liu, X.-F. Li, Z.-X. Guo, Y.-Z. Li, A.-J. Huang, W.-B. Chang, J. Mol. Catal. A: Chem. 179 (2002) 27.
[3] J.T. Groves, Y. Watanabe, J. Am. Chem. Soc. 108 (1986) 7836.
[4] K.A. Jorgensen, J. Am. Chem. Soc. 109 (1987) 688.
[5] P. Battioni, J.P. Renaud, J.F. Bartoli, M.R. Artiles, M. Fort, D. Mansuy, J. Am. Chem. Soc. 110 (1988) 8463.
[6] A.M.R. Gonsalves, R.A. Johnstone, M. Pereira, J. Shaw, A.N. Sobral, Tetrahedron Lett. 32 (1991) 1355.
[7] M.J. Nappa, C.A. Tolman, Inorg. Chem. 24 (1985) 4711.
[8] D. Mansuy, J.-F. Bartolli, M. Momenteau, Tetrahedron Lett. 23 (1982) 2781.
[9] J.T. Groves, R.S. Myers, J. Am. Chem. Soc. 105 (1983) 5791.
[10] P.S. Traylor, D. Dolphin, T.G. Traylor, J. Chem. Soc., Chem. Commun. (1984) 279.
[11] B.R. Cook, T.J. Reinert, K.S. Suslick, J. Am. Chem. Soc. 108 (1986) 7281.
[12] D. Ostoviæ, T.C. Bruice, J. Am. Chem. Soc. 111 (1989) 6511.
[13] Y. Iamamoto, M. Assis, K.J. Ciuffi, H.C. Sacco, L. Iwamoto, A.J. Melo, O.R. Nascimento, C.M. Prado, J. Mol. Catal. A: Chem. 109 (1996) 189.
[14] Y. Iamamoto, K.J. Ciuffi, H.C. Sacco, L.S. Iwamoto, O.R. Nascimento, C.M. Prado, J. Mol. Catal. A: Chem. 116 (1997) 405.
[15] P.R. Cooke, J.R.L. Smith, J. Chem. Soc., Perkin Trans. 1 (1994) 1913.
[16] P. Battioni, J.-P. Lallier, L. Barloy, D. Mansuy, J. Chem. Soc., Chem. Commun. (1989) 1149.
[17] J.A.S. Razenberg, A.W. Van der Made, J.W.H. Smeets, R.J.M. Nolte, J. Mol. Catal. 31 (1985) 271.
[18] A.W. van der Made, J.W.H. Smeets, R.J.M. Nolte, W. Drenth, J. Chem. Soc., Chem. Commun. (1983) 1204.
[19] C.-J. Liu, W.-Y. Yu, S.-G. Li, C.-M. Che, J. Org. Chem. 63 (1998) 7364.
[20] B.-Z. Zhan, X.-Y. Li, Chem. Commun. (1998) 349.
[21] T.A. Khan, J.A. Hriljac, Inorg. Chim. Acta 294 (1999) 179.
[22] I.L.V. Rosa, C.M. Manso, O.A. Serra, Y. Iamamoto, J. Mol. Catal. A: Chem. 160 (2000) 1999.
[23] D.F. Zinkel, J. Russel, Naval Stores, Pulp Chemical Association, New York, 1989.
[24] R.S. Dowining, H. van Bekkum, R.A. Sheldon, CATTECH 95, December 1997.
[25] Sopharma USA Coorporation, 2001; http://www.sopharma.com/categories/447/44704rhinolex.html.

[26] (a) O.A. Badary, A.M.E. Din, Cancer Detect. Prev. 25 (2001) 362;
(b) M.-H. Daba, M.S. Abdelrahman, Toxicol. Lett. 95 (1998) 23.

[27] F.S. Vinhado, C.M.P. Manso, H.C. Sacco, Y. Iamamoto, J. Mol. Catal. A: Chem. 174 (2001) 279.

[28] R.R.L. Martins, M.G. Neves, A.J. Silvestre, M.M. Simões, A.M. Silva, A.C. Tomé, J.A. Cavaleiro, P. Tagliatesta, C. Crestini, J. Mol. Catal. A: Chem. 172 (2001) 33.

[29] R.L. Martins, M.G. Neves, A.J. Silvestre, A.M. Silva, J.A. Cavaleiro, J. Mol. Catal. A: Chem. 137 (1999) 41.

[30] A. Thellend, P. Battioni, D. Mansuy, J. Chem. Soc., Chem. Commun. (1994) 1035.

[31] R.M. Liegel, M.Sc. Thesis, University of St. Paulo, Brasil, 1996.

[32] O. Leal, D.L. Anderson, R. Bowman, F. Basolo, R. Burwell, Jr., J. Am. Chem. Soc. 5126 (1975).

[33] G. Engelhardt, D. Michel, High-Resolution Solid-State NMR of Silicates and Zeolites, Wiley, USA, 1987 (Chapter V).

[34] D.W. Breck, Zeolite Molecular Sieves, Krieger Publishing Company, USA, 1984.

[35] J.-P. Renaud, P. Battioni, J.F. Bartoli, D. Mansuy, J. Chem. Soc., Chem. Commun. (1985) 888.

[36] P.L. Anelli, S. Banfi, F. Montanari, S. Quici, J. Chem. Soc., Chem. Commun. (1989) 779.

[37] S. Banfi, A. Maiocchi, A. Moggi, F. Montanari, S. Quici, J. Chem. Soc., Chem. Commun. (1990) 1794.

[38] P.J. Kunkeler, J.C. Van der Waal, J. Bremmer, B.J. Zuurdeeg, R.S. Dowing, H. Van Bekkum, Catal. Lett. 53 (1998) 135.

[39] M. Milos, Appl. Catal. A: Gen. 216 (2001) 157.

[40] K. Tomizawa, Y. Ogata, J. Org. Chem. 46 (1981) 2107.

[41] J.O. Edwards, R. Curci, in: G. Strukul (Ed.), Catalytic Oxidations with Hydrogen Peroxide as Oxidant, Kluwer Academic Press, Dordrecht, 1992.

[42] D.R. Leanord, J.R.L. Smith, J. Chem. Soc., Perkin Trans. 2 (1991) 25.